Jour. Geol. Soc. India (2022) 98:883-892
https://doi.org/10.1007/s12594-022-2091-1

ORIGINAL ARTICLE

Petro-physics Analysis and Rock Physics Modeling for Estimation of Gas Hydrate Saturation: A Case Study in the Mahanadi Offshore Basin

Pradeep Kumar Shukla[1], Dip Kumar Singha[1,2*], Pradeep Kumar Yadav[1]and Kalachand Sain[3]

[1]Department of Geophysics, Institute of Science, BHU, Varanasi - 221 005, India
[2]Department of Geology and Geophysics, IIT, Kharagpur - 721 302, India
[3]Wadia Institute of Himalayan Geology, Dehradun - 248 001, India
***E-mail:** dipgeo89@gmail.com; dipks21@gg.iitkgp.ac.in*

Received: 17 September 2021 / Revised form Accepted: 1 February 2022

ABSTRACT

Gas hydrate saturation (S_h) is the most challenging key parameter of petrophysical evaluations for reservoir characterization. In total three wells were used (namely, NGHP-01-19, NGHP-01-09, and NGHP-01-08) to compute the petrophysical parameters in the gas hydrate-bearing sediments of the Mahanadi offshore basin. Initially, effective porosity and volume of shale are computed using conventional log data varying from 11-36% and 55-75% respectively. The most prominent technique responding to the physical property has been used to compute the S_h by using Archie's empirical electrical resistivity method. The presence of gas hydrate, free gas, and other lithology affects the sonic velocity which is widely used to quantify the hydrate saturation. Therefore, an attempt is made to quantify the S_h from the wellbore sonic velocity using a rock physics model at higher porosity (~62%) for unconsolidated marine sediments below the seafloor. The model is best suited for gas hydrate zones where velocity increases with the hydrate saturation but underestimates the saturation for free gas zones below the bottom simulating reflector. In the study area, S_h ranges from 5-13% in the depth interval of 175-200 mbsf for well NGHP-01-19 whereas, small amount of 3-10% and 2-8% for well NGHP-01-09 and NGHP-01-08 respectively. The S_h obtained from the rock physics model is insignificantly mismatched with the saturation obtained from temperature and resistivity data due to the presence of an isotropic layer with fracture filling sediments having anisotropic properties.

INTRODUCTION

Gas hydrate is occurring in solid crystalline structure with some guest molecules mostly methane gas entrapped in hydrogen bonding water lattice (Sloan, 1998, Sain and Gupta, 2012). It mostly occurs in shallow regions of the outer continental margin of deep offshore basins. The gas hydrates are found in probable temperature (<10°C) and pressure (> 0.6 MPa) conditions. It is also inferred by a typical seismic bottom simulating reflector (BSR), cross-cutting channels, and seismic amplitude attenuation or blanking using high resolution multichannel seismic (MCS) data (Sain and Gupta, 2012, Coffin et al., 2007). The gas hydrate sediments show relatively higher seismic velocity than that of surrounding sediments while the gas hydrates occur mostly in fracture filings, veins, and pore filling of the shallow marine sediments in the study area of the offshore Mahanadi basin (Singha et al., 2019). Gas hydrate generally shows high elastic moduli than other pore-filling fluids and hence acoustic wave velocity increases in gas hydrate-bearing sediments (Stoll and Bryan, 1979, Tucholke et al., 1977). Based on that assumption, several rock physical models have been theorized for the computation of gas hydrate saturation. The assessment of a gas hydrate reservoir is done by computing petrophysical parameters such as water saturation, effective porosity, and volume of shale. The petrophysical parameters especially water saturation and porosity both have been derived from the seismic velocity (P- and S- wave) using the rock physics model. Therefore, the accuracy of the estimation of the parameters depends on the seismic velocity which is greatly influenced by porosity, lithology, burial depth and other geological factors (Mavko et al., 2009; Lee and Collett, 2012; Shukla et al., 2022a). Several authors, namely, Gosh et al. (2010), Kumar et al., (2006), Lee and Collett (2011), Waite et al., (2019), Cook et al., (2008) and Shankar and Pandey (2016) have previously reported the fracture filling gas hydrate in both the basin Krishna-Godavari (K-G) and Mahanadi offshore basin respectively. For accurate assessment and characterization of gas hydrates from seismic velocity and other rock properties in the Mahanadi offshore basin, Logging While Drilling (LWD) techniques acquired a continuous record of various geo-physical parameters of sediments with respective depths of the wellbore. The measurements of such physical properties from P-wave velocity, resistivity, density, porosity, gamma-ray, and volume of shale have been used in this study. Among all measurable physical parameters, electrical resistivity is found to be one of the most sensitive measurements to the presence of gas hydrates. In the presence of gas hydrate, both the P-wave velocity and resistivity relatively increase in the gas hydrate concentration, while density relatively decreases (Lee and Collett, 2012). The density log has been used to obtain the porosity previously reported (Singha et al., 2019; Shukla et al., 2022b) for estimation of Archie's parameters and, it has also been used in the rock physics model. However, the porosity can't be treated as prior information for gas hydrate concentration as a caliper log is used to measure the relative borehole size and gamma-ray is used for the detection of lithologies readings which are not direct indicators of gas hydrates (Serra, O., 1984). Gas hydrate studies carried out by National Gas Hydrate Program Expedition 01 introduced the gas hydrates mainly in fractured clay-rich sediments (Collett et al., 2014; Pandey et al.,

2019) in K-G Basin. Gas hydrate bearing sediments were identified in the Mahanadi and Andaman basins (Collett et al., 2014). Various models have been carried out for computation of the gas hydrate saturations using P-wave velocities and porosity such as the Wood equation (Wood et al., 1994; Nobes et al., 1986), modified Hashin-Shtrikeman (H-S) model (Dvorkin et al., 1999), Biot-Gassmann, weighted average equations (Lee et al., 1996; Collett, 2001; Ojha and Sain, 2007), and the time average equation (Miller et al., 1991; Lee et al., 1996). If gas hydrate occurs in sand-dominated sediments, the physical properties of hydrate-bearing sediments reveal isotropic nature and if they are present in fractures of fine-grained sediments, the physical properties reveal an anisotropic nature (Sayers and Kachanov, 1995; Lee and Collett, 2011; Shukla et al., 2022a). In this paper, the aim is to focus on petrophysical parameters analysis using conventional well log data such as sonic, density, resistivity, and gamma-ray log and further estimation of gas hydrate saturation by using Archie's empirical electrical resistivity method and the rock physical model. In the rock physics model, the modified H-S upper model has been considered for the computation of gas hydrate saturation. Wood's equation is applied to compute saturation and compared with modified H-S upper bound model. The gas hydrate saturation from both models has been further validated with gas hydrate saturation which is computed from electrical resistivity methods. Gas hydrates saturation from electrical resistivity log data using Archie's (1942) empirical relation and rock physics model using a two-phase effective elastic medium which is suitable for high porosity sediments with gas hydrate and free gas.

GEOLOGICAL SETTING OF STUDY AREA

This study area is basically located at the northern part of the passive eastern continental margin of India (ECMI). It covers mainly sediment deposited from discharge by two rivers namely Mahanadi and Krishna-Godavari river (Sastri et al., 1981). In the of ECMI, the offshore Mahanadi basin is surrounded by the K-G basin in the south west direction and, the bay of Bengal basin in the north east direction and its covering an area of 14,000 sq. km (Bastia et al., 2010) as shown in Fig.1. The basin evolved due to rifting and break-up of Gondwana supercontinent land during permo-triassic geological age (Sastri et al., 1981, Sastri et al., 1973). Due to collision of Indian plate and Eurasian plate during Miocene, sediments thickness developed by 8 km from upper Cretaceous to recent geological age in this offshore basin (Fuloria et al., 1992).Source rock studies on drill cuttings and sidewall cores from the wells drilled in shallow offshore indicate presence of adequate total organic carbon (TOC 1.5-2.5%). Additionally, organic matter within the Paleocene and older sediments appear to be mature. This observation suggests that better source sediments can be present in the deeper parts of the basin. The organic matter in the Paleocene and older sediments shows marginally maturity. TOC values of more than 3% also have been recorded in some samples (Sain et al., 2011, Kumar et al., 2014). Although high TOC, abounded deposition rate of sedimentations (20-40 cm/kyr) and geothermal gradients of 35-45°C/km may suggest the indication of gas hydrate reservoir in the deep offshore basin wherever low temperature and high pressure assure the complimentary environments in the basin (Singh et al., 2019, Sain et al., 2011, Shankar et al., 2013, Kumar et al., 2014 and Collette et al., 2008).The indication of gas hydrates are also recognized by LWD and temperature of core sample by infrared ray (IR) camera at NGHP-01 sites in the offshore Mahanadi basin (Kumar et al., 2014, Rai et al., 2020, Sain and Gupta, 2012; Shukla et al., 2022a and Shukla et al., 2022b). Overall from these studies it shows that migratory hydrocarbons are present and, gas hydrate due to high impermeable porous rock in the Miocene and older sediments of Mahanadi offshore basin. Gas hydrates deposition of clay/silt sediments with fractures in the deep water basin of Pleistocene age.

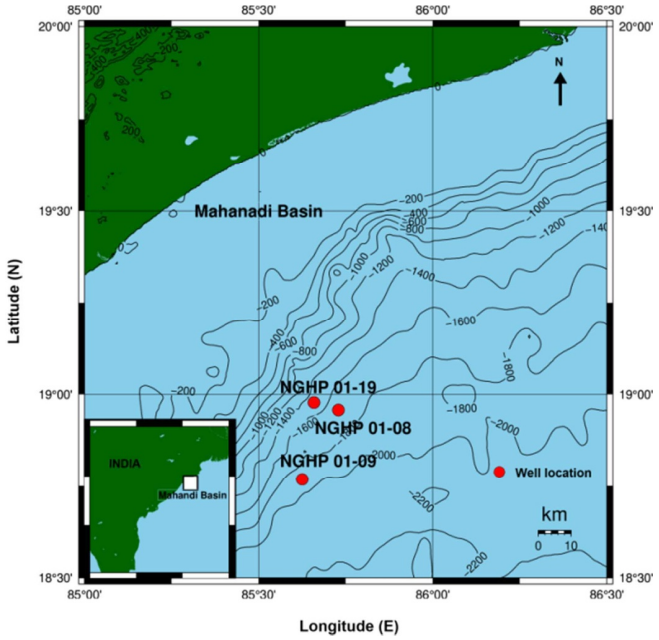

Fig. 1. Depicted bathymetric map of study area at drill site over offshore Mahanadi basin for NGHP-01-19, NGHP-01-09 and NGHP-01-08 respectively.

THEORY AND METHODOLOGY

Well Log Data Analysis

Initially, P-wave velocity and resistivity logs are used to infer the gas hydrate concentration while the density and gamma-ray logs can't be treated as direct substitutes for the gas hydrate concentration. The P-wave increases at the gas hydrate stability zone (GHSZ) and shows a sudden decrease just below the GHSZ. The gamma-ray log is used to infer lithological variations in terms of clay-rich or mud-rich shale. The gas hydrate zone and free gas zones can be identified from the initial well log data analysis as listed in table1. The depths of BSR are 208, 290, and 257mbsf, and the depths of the seafloor are 1433, 1935, and 1701m for wells NGHP-01-19, NGHP-01-09, and NGHP-01-08 respectively. The inclusion of gas hydrate in voids of marine sediments significantly affects the bulk electrical properties of sediments and measurement of such properties can be directly used for the estimation of gas hydrate saturation (Pandey et al., 2019). Based on electrical resistivity log data, the water-saturated sediments have less resistivity as compared to true or bulk resistivity as sediments containing gas hydrates as just above the BSR and free-gas below the BSR. This difference in recorded resistivity log values can be used to calculate the gas hydrate saturations (e.g. Collett and Ladd, 2000, Lee and Collett, 2012). After detailed analysis of well log data for the occurrence of gas hydrate; our next aim is to evaluate the petrophysical parameters like effective porosity, the volume of shale, and gas hydrate saturation from Archie's empirical relation and rock physics models by following the flowchart as shown in Fig. 2.

Here, these are the basic steps for the computation of the gas hydrate saturation using modified H-S model as follows:

- Initially, using (Hill, 1952) average formula, the bulk (K_{matrix}) and shear moduli (G_{matrix}) of the rock matrix are determined using equation (16, and 17) in table (2) (Helgerude, 1999).
- Using rock matrix bulk and shear moduli, elastic moduli of dry rock (K_{HM}, and G_{HM}) at critical porosity (ϕ_c) is determined from Hertz-Mindlin model from equation 10 (a, and b)
- Using elastic moduli of Hertz-Mindlin model, elastic moduli of dry rock (K_{dry} and G_{dry}) are determined for various porosities

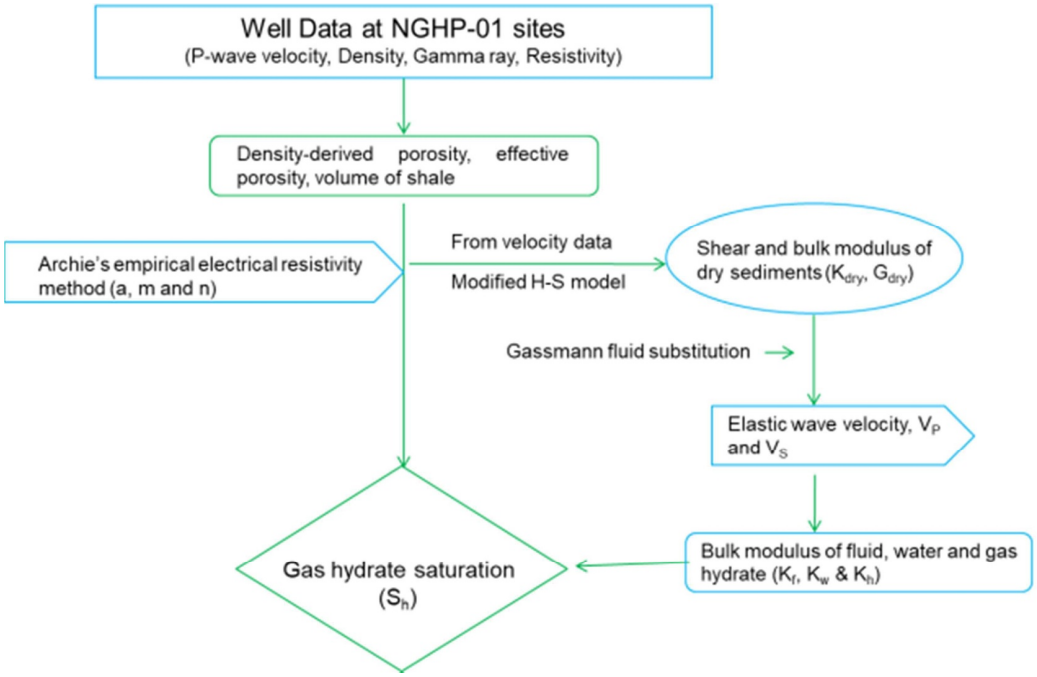

Fig. 2. Flow chart of estimating effective porosity, volume of shale and, gas hydrate saturation using Archie's equation and rock physics model.

(0-100%) of the rock using equation (7a, and 7b) and equation (8a and 8b)

- Saturated bulk modulus (K_{sat}) of the rock is determined using sonic P-wave velocity.
- Substituting values of various parameters like porosity, K_{dry}, K_m and K_{sat} in Gassmann equation (Gassmann 1951), hence bulk modulus of the fluid (K_f) is determined from equation (13)
- K_f is the bulk modulus of the homogeneous mixture of water and gas hydrate and further the saturation of water is determined using equation (19)
- Finally, the gas hydrate saturation is computed by using equation (20)

Estimation of volume of shale and effective porosity:

The determination of reservoir quality in terms of petrophysical parameters, lithology identification, porosity, type and distribution of reservoir fluids are based essentially on the evaluation of shale volume (V_{Shale}). Since these above parameters are most important to the proper evaluation of reservoir potentiality. Therefore, to quantitatively evaluate a formation, there are precisely estimated volume of shale for effective porosity and gas hydrate saturation. The V_{Shale} distribution is one of the most prominent factors that have to be considered in petrophysics and formation evaluation. The volume of shale is used to determine from gamma ray log as given by following standard equation (Fertl and Frost, 1980);

$$V_{Shale}\,(\%) = \frac{GR_{log} - GR_{min}}{GR_{max} - GR_{min}} \times 100 \qquad (1)$$

Where, GR_{log} is the gamma-ray response in the zone of interest, GR_{min}= 30API is the gamma-ray response in cleanest formation, GR_{max} = 150 API is the gamma-ray response in the shale layer.

Accordingly, the rock can be differentiated as clean if V_{Shale}< 10%; shaly if V_{Shale} ranged from 10% to 33%, and if the V_{Shale} is more than 33%, it is considered to be shale. The volume of shale at site NGHP-01-19 is 55% in the depth interval of 175-200m. Similarly, the volume of shale is 65% and 70% in the depth interval of 265-290mbsf and 235-257mbsf for the well NGHP-01-09 and NGHP-01-08 respectively.

Due to the unavailability of any core data to calibrate and evaluate the density-derived porosity, the LWD log-derived density measurements ($\tilde{n}_b$) were used to calculate sediment effective porosity (ϕ_E) as given by Adolph et al., 2005;

$$\phi_E = (1 - V_{shale}) * \phi \qquad (2)$$

Where, ϕ is the density-derived porosity. The effective porosity values computed from using above equation (2) are varying from 20-40%, 15-34% and 11-23% in 25m of gas hydrate zone in the depth intervals of 175-200mbsf, 260-285mbsf and 225-250mbsf consequently 36-27%, 17-38% and 9-26% in free gas zone as illustrated in Table1. Finally, the representation of P-wave velocity, density, gamma-ray, resistivity, effective porosity, and volume of shale are plotted as shown in Fig. 3(a b and c) respectively. We have identified the BSR from multi-channel seismic data and, the depth of BSR in each well has been estimated by seismic well tie correlation and as well as by the geophysical data such as velocity, resistivity and temperature log described in (Sain et al., 2011; Singha et al., 2019; Shukla et al., 2022a; Shukla et al., 2022b).

Gas Hydrates Saturation from Electrical Resistivity Log Data using Archie's Relation

For accurate and better assessment of the gas hydrate saturation in uncompacted shale and porous medium, we have to apply the well-known Archie's empirical relationship in order to resistivity and porosity logs recorded for well NGHP-01-19, NGHP-01-09 and NGHP-01-08 respectively in the offshore basin. The pore fluid resistivity (R_w) was estimated from Fofonoff (1985) using a linear temperature profile derived from the *in situ* temperature measurements as follows;

$$R_{W2} = R_{W1}\,\frac{T_1 + 21.5}{T_2 + 21.5} \qquad (3)$$

Here, T_1 is the seafloor temperature (4.78 °C);T_2 is the temperature (°C) of formation at depth of wellbore and geothermal gradient of

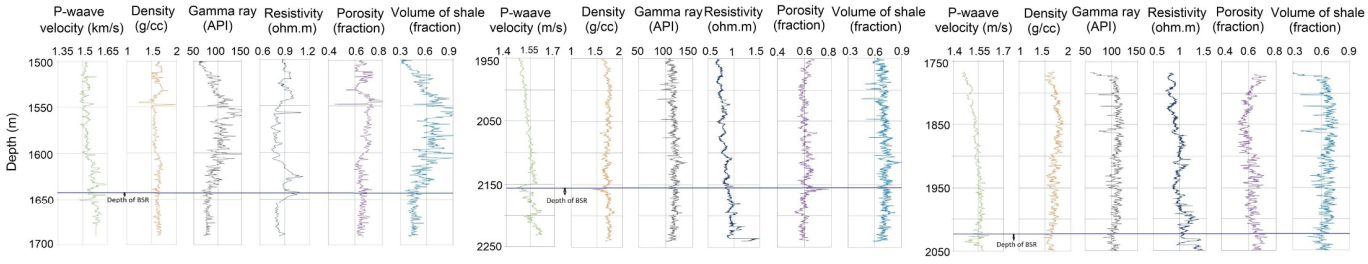

Fig. 3. Conventional well log data such as P-wave velocity, density and resistivity with petrophysical parameters such as porosity, volume of shale and gamma ray for well **(a)** NGHP-01-19. **(b)** NGHP-01-09 and **(c)** NGHP-01-08 respectively.

sediment in offshore Mahanadi basin is 52.3°C/km (Collett et al., 2008) as given;

$$T_2 = (\text{Geothermal gradient}) * \text{depth} + T_1$$

Formation factor (FF) is defined by the ratio of resistivity of 100% water saturated sediments or background resistivity (R_0) to R_w (= R_{W2}). The R_{W1} and R_{W2} is the resistivity of water at the surface of seafloor and temperature derived resistivity throughout the well respectively in this study area. Since R_W and R_{W2} both are equal i.e. $R_W \sim R_{W2}$. So, we have computed R_{W2} using equation (3) after that applied to equation (4) for other relevant component which were required for gas hydrate saturation. The least square power law fit with depth of the values measured on pore water samples is as follows (Archie, 1942and 1952)

$$\text{Where,} \quad FF = R_0/R_W = R_0/R_{W2} = a/\varphi^m, \tag{4a}$$

Taking log bot side we get,

$$\text{Log FF} = -m \text{ Log } \phi + \text{Log a}$$
$$\text{Or, FF} = \text{antilog } (-m \text{ Log } \phi) + \text{antilog (Log a)} \tag{4b}$$

The necessity of porosity-formation factor to find the Archie's constant such as a, m, and n. Here, *a* is the tortuosity factor, *m* is the cementing exponent of rock, and *n* is the saturation exponent (taken usually close to 2). We have plotted a crossplot with logarithm equation between formation factors (FF) to density-derived porosity for water-bearing sediments (Non-hydrate zone) to find the Archie's constant (especially a, and m) .The constants in the equation depend on interaction between the host sediments and gas hydrate in a porous medium. Firstly, for computation of the Archie constants, we assume R_0 is very close to the bulk or true resistivity, R_t. Since resistivity log and porosity log curve is mirror to each other so, predicted R_0 derived from equation (4a) using the porosity log and Archie's equation i.e. $R_0 = (aR_w)/\varphi^m$. A linear fit straight line represent best-fit matches using equation (4b) between FF and porosity is plotted by trial and error method, we optimized the values of Archie constants which are as follows; a = 2.3 and m = 0.75 for well NGHP-01-19. Similarly, a = 1.90 and m =1.2 for well NGHP-01-09 and a = 1.91 and m = 2.3 for well NGHP-01-08 respectively as shown in figure 4 (a, b and c) and Table 1. The estimated water saturation, assumed to be the numerical complement of the hydrate saturation as given by (Archie, 1942 and 1952)

$$S_h = 1 - (R_0/R_t)^{1/n}, \tag{5}$$

The computed water-saturated resistivity is very close to the measured resistivity as the water saturation is close to 100% above ~180, ~260 and ~220 mbsf. Below this depth, the results suggest that as much as 10% of the pore space could be occupied either by gas hydrate above the BSR (estimated at ~208, 290 and 257mbsf).

The downhole profile of the hydrate saturation from resistivity method provides 8-12%, 6-10% and 2-5% of the gas hydrates saturation at the depth interval of 175-200m, 260-285m and 225-250m below sea floor in the wells. The representation of computed gas hydrate and free gas saturation using resistivity method has been plotted in the later section as shown in Fig.12 (a, b and c) for wells NGHP-01-19, NGHP-01-09 and NGHP-01-08 respectively.

As previously, we derived the predicted R_0. A qualitative influence of gas hydrate on the resistivity log is indicated by the difference between R_0 and R_t as shown in Fig. 5 (a, b, and c). The deviation between R_0 and R_t clearly indicates the presence of the gas hydrates in the sediments. The gas hydrate saturation ranges from 5-10% as derived from infrared imaging log and the lower temperature value that shows the presence of the gas hydrate in the depth range of 175-200mbsf for the well NGHP-01-19 respectively as shown in Fig.6.

Gas Hydrate Saturation using Effective Medium Rock Physics Model

Rock physics models are being used indirectly for estimation of

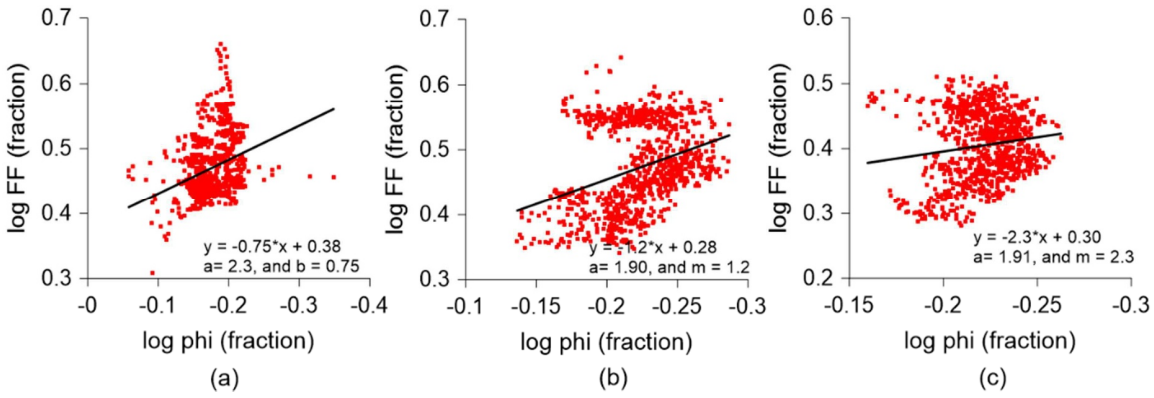

Fig. 4. Computing Archie's constant such as a, and m using linear best fit logarithm plot between Formation factor, FF (unit less) and porosity (fraction) for wells NGHP-01-19, NGHP-01-09 and NGHP-01-08 respectively.

Table 1. Illustrate table for well data analysis, Archie's constant and volume of shale, effective porosity and resistivity at NGHP-01 sites in the study area.

Wells	BSR depth (mbsf)	Seafloor depth (m)	Gas hydrate zone (mbsf)	Archie's constant a	m	n	Volume of shale (%)	Effective porosity (%)	Resistivity, R_t (Ohm. m)
NGHP-01-19	208	1433	175-200	2.3	0.75	2	55	20-40	0.88-1.12
NGHP-01-09	290	1935	260-285	1.90	1.2	2	65	15-34	0.95-1.36
NGHP-01-08	257	1701	225-250	1.91	2.3	2	70	11-23	0.76-0.98

the gas hydrate using elastic parameters and velocity information for several values of the gas hydrate saturation and the best fitting model gives the saturation of the gas hydrate in the pores of sediment. We used some of these models to estimate the saturation of gas hydrate and free gas sediments discussed below.

Wood's Model

The Wood's (1941) method is the primary approach to compute

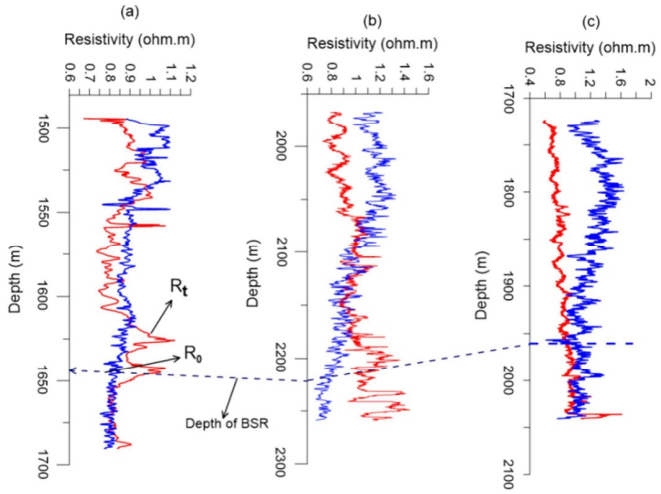

Fig. 5. Separation between bulk resistivity R_t in red and calculated water saturated resistivity R_0 in blue indicating the presence of gas hydrate for well **(a)** NGHP-01-19, **(b)** NGHP-01-09, and **(c)** NGHP-01-08 respectively

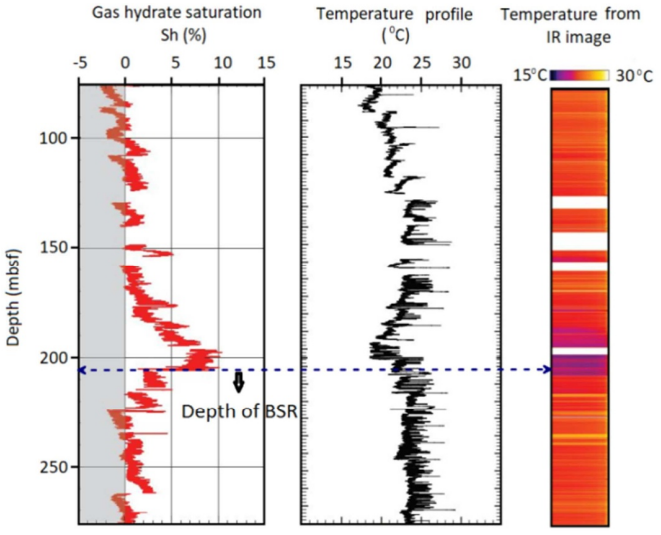

Fig. 6. Estimate of gas-hydrate saturation abundance and the derived downhole temperature profile relates with Infrared imaging indicating the presence of gas hydrate in the depth range of 183-208mbsf with low temperature for corresponding depth range for well NGHP-01-19.

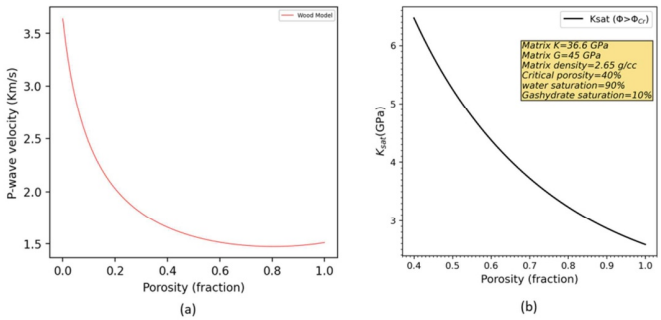

Fig.7. Theoretical plot for the rock physics models **(a)** Wood's model and **(b)** modified H-S upper model for matrix bulk, shear modulus and density for quartz for critical porosity at 40% with water saturation 90% and gas hydrate saturation 10% respectively (Wood, 1941; and Dvorkin et al., 1999)

the in-situ gas hydrate saturations. It is used in a highly porous medium and loose sedimentary formation where gas hydrate is a part of fluid suspension as followed by,

$$\frac{1}{\rho_b V_p^2} = \frac{\phi(S_h)}{\rho_h V_h^2} + \frac{\phi(S_w)}{\rho_w V_w^2} + \frac{(1-\phi)}{\rho V^2} \quad (6)$$

Where V is the velocity of P-wave in rock matrix; V_p is the P-wave velocity of the hydrate-bearing sediments; V_W is the velocity of fluid, S_w is the water saturation.

The computed gas hydrate saturation (>15%, >10%, and >5%)

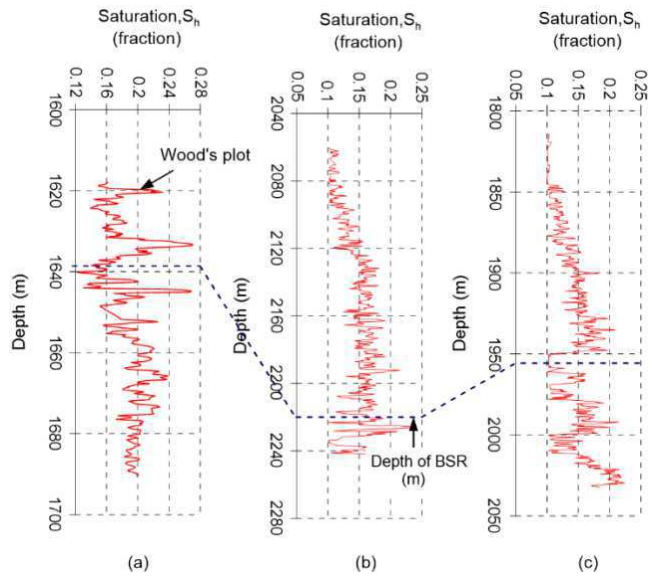

Fig.8. Estimation of gas hydrate saturation considered to be overestimated from sonic velocity using the Wood's model for well **(a)** NGHP-01-19 **(b)** NGHP-01-19, and **(c)** NGHP-01-08 respectively showing higher values above BSR.

from Wood's model as shown in Fig.8 (a, b and, c) and further validated with reported temperature profile core data and Archie's empirical electrical resistivity method that gives that the gas hydrate saturation is not more than 15%, 10% and 5% at wells NGHP-01-19, NGHP-01-09, and NGHP-01-08 respectively.

Wood's model gives overestimated results of gas hydrate saturation in this study area that's why we considered only the modified H-S lower and upper model.

Modified H-S model

The baseline model for estimation of gas hydrate saturation has initially given by Dvorkin et al. (1999) i.e. the modified H-S lower and upper model, which expresses the bulk (K_{dry}) and Shear (G_{dry}) moduli of dry sediments as:

$$K_{dry} = \left[\frac{\phi / \phi_c}{K_{HM} + (4/3)G_{HM}} + \frac{1 - (\phi / \phi_c)}{K_{HM} + (4/3)G_{HM}} \right]^{-1} - (4/3)\, G_{HM}$$

When $\phi < \phi_c$ (7a)

$$K_{dry} = \left[\frac{(1 - \phi) / (1 - \phi_c)}{K_{HM} + (4/3)G_{HM}} + \frac{(\phi - \phi_c)/(1 - \phi_c)}{(4/3)G_{HM}} \right]^{-1} - (4/3)\, G_{HM}$$

When $\phi \geq \phi_c$ (7b)

and,

$$G_{dry} = \left[\frac{\phi /\phi_c}{G_{HM} + Z} + \frac{1 - (\phi /\phi_c)}{G + Z} \right]^{-1} - Z \quad \text{When } \phi < \phi_c \quad (8a)$$

$$G_{dry} = \left[\frac{(1 - \phi) / (1 - \phi_c)}{G_{HM} + Z} + \frac{(\phi - \phi_c)/(1 - \phi_c)}{Z} \right]^{-1} - Z$$

When $\phi \geq \phi_c$ (8b)

Where

$$Z = \frac{G_{HM}}{6} \left[\frac{9\, K_{HM} + 8\, G_{HM}}{K_{HM} + 2\, G_{HM}} \right] \quad (9)$$

$$K_{HM} = \left[\frac{n^2 (1 - \phi_c)^2 G^2 P_{eff}}{18\pi^2 (1 - v)^2} \right]^{1/3} \quad (10a)$$

$$G_{HM} = \frac{(5 - 4v)}{5(2 - v)} \left[\frac{3n^2 (1 - \phi_c)^2 G^2 P_{eff}}{2\pi^2 (1 - v)^2} \right]^{1/3} \quad (10b)$$

ϕ_c is the critical porosity basically considered 40% for high porous unconsolidated bearing gas hydrate sediments; P_{eff} is the effective pressure which is the difference between vertical stress and hydrostatic/or pore pressure (Dvorkin et al., 1999). The pore pressure gradient is 10.11 MPa/km and vertical stress gradient is 10.67 MPa/km (Singha et al., 2019). After subtraction of pore pressure from vertical stress, we got the effective stress which is used in the equation (10a and 10b); K_{HM} and G_{HM} are bulk and shear moduli of the rock matrix which are given by Hertz-Mindlin respectively and n is the average number of contacts per grain in a sphere pack at porosity ϕ, which can be calculated by the following empirical relation (Murphy, 1982).

$$n = 20 - 34\phi + 14\phi^2, \quad (11)$$

and, v is the Poisson's ratio of rock matrix given by

$$v = \frac{(1/2)\,(K - (2/3)\, G)}{K + (1/3)\, G} \quad (12)$$

Using above equations we have computed bulk and shear modulus for dry sediments. The elastic moduli of the rock matrix are dependent on the elastic moduli of the constituent minerals of the rock and their respective volumetric fraction in the rock (Helgerud et al., 1999). Elastic parameters of different constituents of the rock matrix and fluid are shown in Table 2. Rock which is assumed to be composed of clay and quartz minerals and the bulk and shear moduli of the rock matrix is used to calculate the saturation from P-wave and S-wave velocity by using equations (14) and (15) respectively. These results were further applied for hydrate saturation by using Gassmann fluid substitution.

Gassmann Fluid Substitutions

For the saturated rock, bulk modulus is obtained from Gassmann fluid substitution equation as given by Gassmann (1951) as follows:

$$K_{sat} = K \frac{\emptyset K_{dry} - \frac{(1 + \emptyset) K_f K_{dry}}{K} + K_f}{(1 - \emptyset) K_f + \emptyset K - \frac{K_f K_{dry}}{K}} \quad (13)$$

Where, K_f is the bulk modulus ofthe fluid.

Because fluids do not have shear strain, shear waves cannot pass through the fluid. Hence shear modulus of dry rock and shear modulus of the saturated rock from equations 7 (a, b) and 8(a, b) are equal.

$$G_{sat} = G_{dry}$$

Once the elastic moduli are known, elastic wave velocities are calculated by:

$$V_p = \sqrt{\frac{K_{sat} + (4/3)\, G_{dry}}{\rho_b}} \quad (14)$$

and,

$$V_s = \sqrt{G_{dry} / \rho_b} \quad (15)$$

In case of a mixed mineralogy, the effective elastic constants of the solid phase are calculated from individual mineral constituents using Hill (1952) average formula:

$$K = 1/2\, [(\Sigma f_i / K_i)^{-1} + \Sigma f_i K_i] \quad (16)$$

$$G = 1/2\, [(\Sigma f_i / G_i)^{-1} + \Sigma f_i G_i] \quad (17)$$

and the mineral density is given by,

$$\rho = \Sigma\, \rho_i f_i \quad (18)$$

Where, f_i, K_i, G_i and ρ_i are volumetric fraction, bulk modulus,

Table 2. Properties of sediment constituents (after Helgrude et al., 1999)

Constituents minerals	Bulk Modulus (GPa)	Shear Modulus (GPa)	Density (g/cc)	P-Wave velocity (km/s)
Clay	20.9	6.85	2.58	3.41
Quartz	36.6	45	2.65	6.04
Brine	2.4	0	1.03	1.5
Methane Hydrate	8.7	3.5	0.92	3.8
Methane Gas	0.1245	0	0.25	0.71

Shear modulus, and density of ith mineral constituent in the mixture.

It is assumed that gas hydrate is the part of pore fluid and does not affect the stiffness of the dry frame of rock. In this case elastic moduli of the fluid (homogeneous mixture of water and gas hydrate) given by Reuss (1929):

$$\frac{1}{K_f} = \frac{S_w}{K_w} + \frac{1 - S_w}{K_h} \tag{19}$$

and finally we get gas hydrate saturation (Sh) as;

$$S_h = 1 - S_w \tag{20}$$

Where, S_w, K_w, and K_h are water saturation, bulk modulus of water and bulk modulus of gas hydrate.

In this case rock matrix is considered to be composed of 10% quartz and 90% shale (based on the gamma ray) and the rock pores are filled with homogeneous fluid with a mixture of water and gas hydrate.

It is found that the resistivity derived gas hydrate saturations relative to pressure core derived gas hydrates saturations are high due to assumption of isotropic conditions in the reservoirs having anisotropic properties. Gas hydrate saturation from the Wood's model gives higher saturation (>15%) than both the modified H-S model and electrical resistivity method but gas hydrate saturation computed from the modified H-S model, and from Archie's empirical relation have approximately in the ranges 5-13 % shows good result and overlapping to each other.

The gas hydrate (or free gas) saturation of wells are estimated from Archie's empirical resistivity method and rock physics models (the modified H-S model) as shown in Fig.9 (a, b, and c)and the results are illustrated as in Table 3 respectively. We have crossplotted between the gas hydrate saturations obtained by Archie and the rock physics model for three wells specially the gas hydrate zones just above the BSR, showing excellent match as shown in Fig.10 (a, b, and c).

Table 3. Gas hydrates saturation with depth for gas hydrate zone (GHZ) and free gas zone (FGZ).

Well Name	Depth range mbsf		From resistivity using Archie's method, Sh (%)		From velocity using rock physics, Sh (%)	
	GHZ (m)	FGZ (m)	GHZ	FGZ	GHZ	FGZ
NGHP-01-19	175-200	208-230	8-12	8-11	5-13	4-11
NGHP-01-09	260-285	290-315	6-10	4-10	3-10	3-12
NGHP-01-08	225-250	257-282	2-5	2-8	2-7	2-9

RESULTS AND DISCUSSIONS

LWD data has been used to distinguish the gas hydrate and free gas saturation in the clay-rich sedimentary basin at three sites drilled in the offshore Mahanadi basin. The GHSZ are lying between 175-200mbsf, 260-285mbsf and 225-250 for above respective wells. The gas hydrate saturation using Archie's electrical method and from the modified H-S model ranges 5-13%, 3-10% and 2-8% in gas hydrate zone of 175-200m, 160-285m, and 225-250m for well NGHP-01-19, NGHP-01-09, and NGHP-01-08 respectively. For proper modeling of the gas hydrate saturation using weighted equation, a modified H-S model equation (10a, and 10b), the value of n needs to be chosen efficiently such that the porosity of the regions is very low; the empirical equation (11) approximates to the modified H-S model and tends

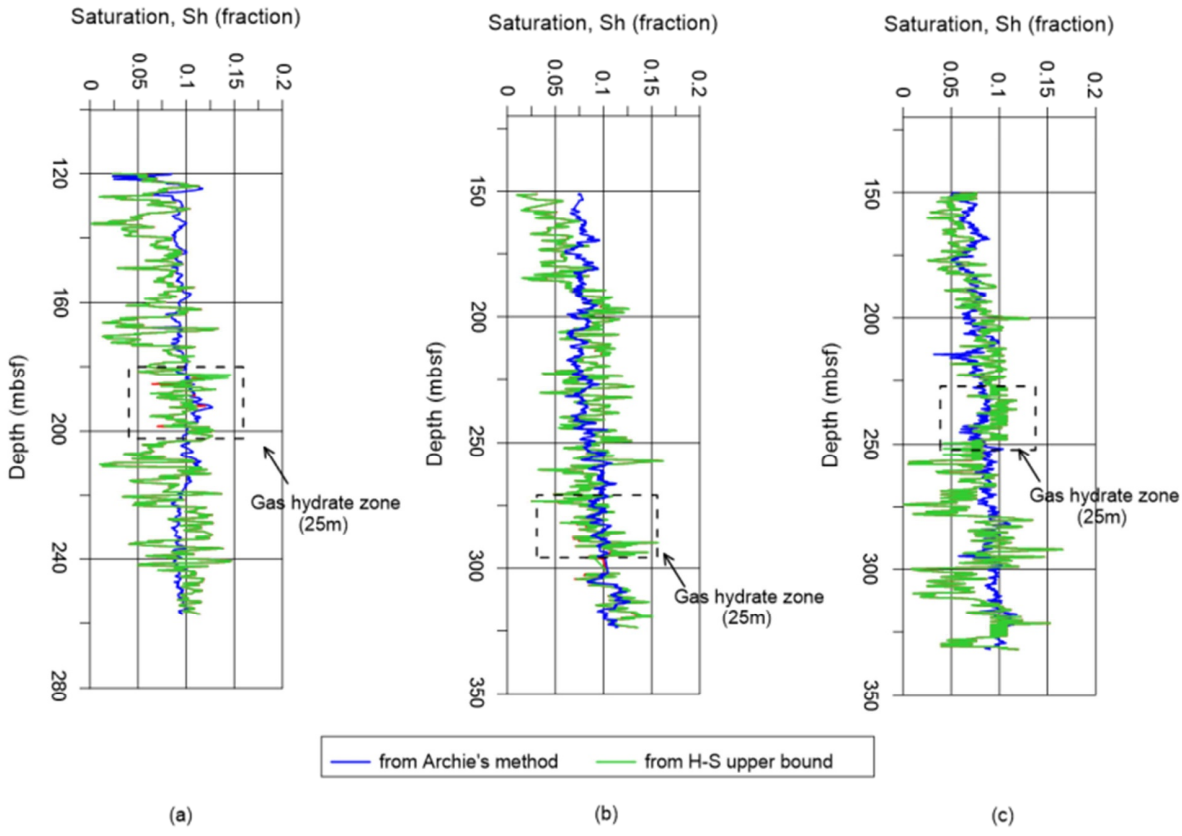

Fig.9. Estimation of gas hydrate saturation from sonic velocity using the rock physics model based on the modified H-S upper bound model ($\phi > \phi_c$), and Archie's electrical resistivity method marked by blue colour shows all are in good correlation for well **(a)** NGHP-01-19, **(b)** NGHP-01-19, and **(c)** NGHP-01-08 respectively.

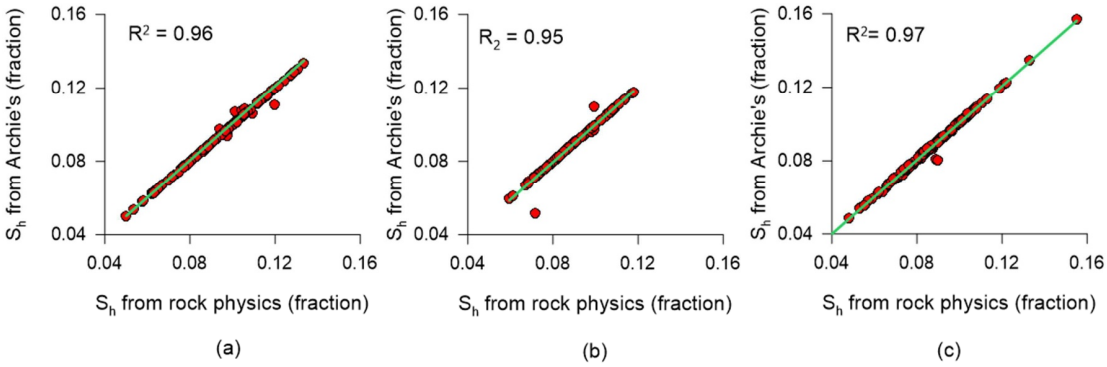

Fig.10. Correlation of gas hydrate saturation obtained from Archie's empirical electrical resistivity method and from the rock physics model (modified H-S model) for well **(a)** NGHP-01-19, **(b)** NGHP-01-09, and **(c)** NGHP-01-08 respectively.

towards Wood's model at high porosity. The predicted velocities at the sites are found to be lower than the actual values. Thus, the velocities estimated by Wood's method do not match the zone where there is no indication of gas hydrate. Due to this reason, Wood's models give overestimated results of the saturation while the modified H-S models gives satisfactory results. Other models like weighted equation and time average equation were not implemented for computing gas hydrate saturation in the study area because they are overestimated compared to the saturation which are obtained by temperature and resistivity data in this uncompacted loose soil mostly contained muds i.e. no cementations between the grains.

The gas hydrate saturations estimated by the Gasmmann equation based on modified H-Supper bound model for porosity higher than critical porosity ($\phi > \phi_c$)are in a very good agreement with the reported value of gas hydrate saturations obtained by temperature profile. Only modified H-S model was considered here because for lower model, the elastic parameters become zero at 100% porosity point (Dvorkin et al., 2019). Hence, according to equations (7a), (7b) (8a) and (8b), the values of K_{dry} and G_{dry} moduli will be equal to K_{HM} and G_{HM} respectively at critical porosity for ($\phi < \phi_c$), and consequently every parameters estimated latter are almost equal at most depths of the wells. Therefore, the estimated gas hydrated (or free gas) saturations are found same. Only the modified H-S upper model gives satisfactory results and approximately overlaps with Archie's electrical method in a ~25m thick zone of the gas hydrate-bearing sediments at NGHP-01-19 site. In Fig.9, the gas hydrate saturation from velocity using the rock physics model shows significant variations in the plot, this reason may be due the presence of gas hydrate pore-filling in the fracture that causes the anisotropy of the velocity in the gas hydrate-bearing sediments.

Variation of Gas Hydrates Saturation with P-wave Velocity

In the rock physics models, especially for the modified H-S models, gas hydrate concentration increases linearly with the increase of velocity and decreases in free gas model because stiffness of free gas is higher than the gas hydrate concentration. A theoretical representation to understand the linear variation of velocity with the hydrate saturation as shown in Fig.11. We prepared this theoretical plot of gas hydrate saturation based on 90% clay and 10% quartz with gas hydrate filled with water for the higher porosity sediments. As for the free gas zone, the velocity drops or decreases, the saturation estimated by the modified H-S model would mislead and underestimate the result.

In thee free gas zone below the BSR, the gas saturations obtained from both methods of the Archie and the rock physics model averagely matched each other because of the presence of shaliness which reduces the resistivity in these zones. The modified H-S models have not accounted for free gas for computation of hydrate saturation; it is only valid for gas hydrate models.

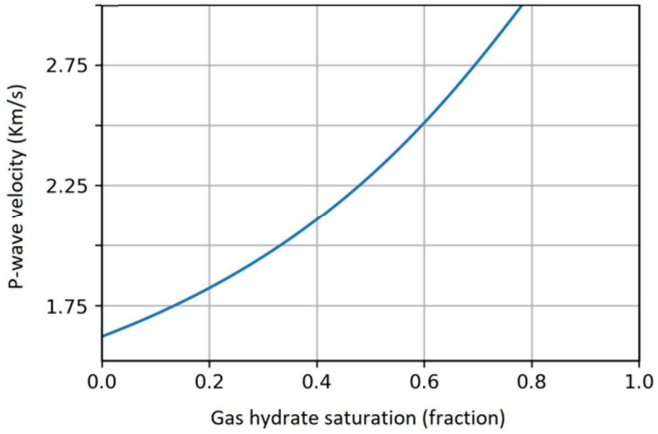

Fig.11. A theoretical plot for understanding the signature of gas hydrate saturation with velocity from gas hydrate model in two phase medium with clay in rock matrix assumed 90% and quartz in rock matrix assumed 10% with porosity of rock 50% with pore filled water and gas hydrate.

VP/VS and P-wave Impedance Characteristic Plot

The crossplot technique of Vp/Vs ratio and P-wave impedance is an important tool to identify the lithology and fluid type in sedimentary rock. The Vp/Vs is the best fluid indicator because it is significantly influenced by the presence of fluid types in the reservoir. As the bulk modulus changes for the presence of water and free gas in a reservoir, the P-wave velocity sharply drops. Due to unavailability of S-wave in other two wells, the cross-plot was done for only NGHP-01-19 well with the colour coded by gamma ray value (API) as shown in Fig.12.

In the study area, the S-wave data are not good quality having lower values, but badly affected by fluid in uncompacted sediments below the seafloor. Therefore, the values of VP|Vs ratio become higher reaching more than 4 to 9 (unitless). Clay/silt, uncompacted shale, gas hydrate and free gas bearing sediments have been identified which is indicated by circles in the Fig.11 based on the ranges of Vp|Vs ratio and P- impedance with comparing conventional log and temperature profile at NGHP-01-19 sites. The P-wave impedance of gas hydrate and free gas-bearing sediments was compared by seismic inverted P-wave impedance reported in (Singha et al., 2019 and Singha et al., 2015).The gas hydrate-bearing sediments having higher P-wave impedance (>2600m/s*g/cc) with VP|VS ratio ranging from 4.23 to 6.02 and gamma ray value (85-115API) marked by red circle for the depth range of 175-200m just above the BSR for well NGHP-01-19 while free gas-bearing sediments with low P- wave impedance value (2420-2637m/s*g/cc) than gas hydrae impedance with low gamma ray value (<100API) and reasonable lower values VP|VS ratio (<4.07)

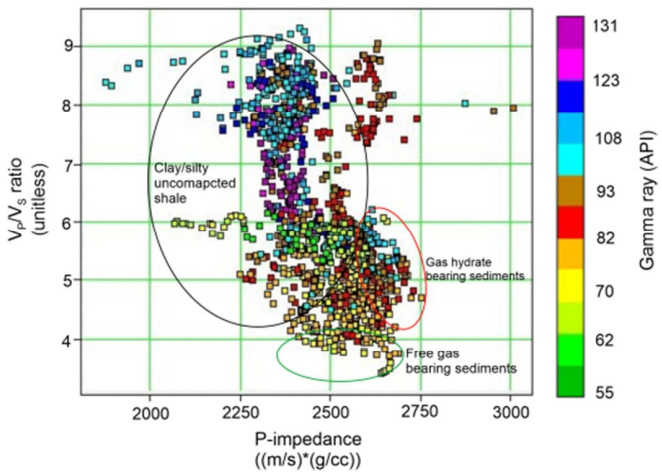

Fig. 12. Depicted cross-plot analysis between Vp|Vs ratio (unitless) and P-wave impedance ((m/s)*(g/cc)) based upon gamma ray (API) value to separate the clay/silt shale, gas hydrate and free gas bearing sediments for the well NGHP-01-19.

just below the BSR marked green circle. A reasonable high value of VP|Vs ratio value (>5) with corresponding wide range of P-wave impedance (<2200m/s*g/cc) at high gamma ray value (>120API) indicates clay/silt uncompacted shale indicted by black circle. The remaining data points may indicate water saturated sediments with clay/silt.

CONCLUSION

The petrophysical parameters like effective porosity, volume of shale and gas hydrate saturation from the well data has been evaluated at NGHP-01 sites. The higher volume of shale indicates clay/silt-rich bearing sediments. The separation of back ground resistivity and true resistivity plot helps to estimate possible thickness of gas hydrate reservoirs above the BSR. Hydrate saturation is computed using Archie's electrical method ranges from 3-12% at site NGHP-01 in high porous uncompacted bearing sediments. The estimated saturation is well matched with saturation obtained by the resistivity data and the infrared temperature in the wells. The modified H-S model for upper bound ($\phi > \phi_c$) gives acceptable ranges of saturation in gas hydrate bearing zone for well NGHP-01-19, NGHP-01-09, and NGHP-01-08 respectively for higher porosity of unconsolidated bearing sediments. The major gas hydrate saturation is observed in NGHP-01-19 site but trace amount of hydrate saturation is observed in the other well sites. The P-wave velocity is affected by lithology and the fluid type. Predicted gas hydrate saturations from Archie's empirical electrical resistivity method and the rock physics model are slightly different because of the isotropic property of pore-filling fracture sediments having anisotropy in nature.

References

Adolph, B. et al. (2005) No more waiting: formation evaluation while drilling. Oilfield Review (Autumn), v.17(3), pp.4-21.

Archie, G.E. (1952) Classification of carbonate reservoir rocks and petro-physical consideration, AAPG Bull., v.36 pp.218-298.

Archie, G.E. (1942) The electrical resistivity log as an aid in determining some reservoir characteristics. Trans. AIME, v.146, pp.54-62.

Bastia, R., Radhakrishna, M., Srinivas, T., Satyabrata Nayak, Nathanial, D.M. and Biswal, T.K. (2010) Structural and tectonic interpretation of geophysical data along the eastern continental margin of India with a special reference to deep water petroliferous basins, Jour. Asian Earth Sci., v.39, pp.608-619.

Collett, T.S., Riedel, M., Cochran, J., Boswell, R., Presley, J., Kumar, P., Sathe, A., Sethi, A., Lall, M., Sibal, V. (2008) The NGHP Expedition 01 Scientists, National Gas Hydrate Program Expedition 01 Initial Reports. Directorate General of Hydrocarbons, Noida and Ministry of Petroleum and Natural Gas, India. 4 Volumes.

Collett, T.S., and Ladd, J. (2000) Detection of gas hydrate with downhole logs and assessment of gas hydrate concentrations (saturations) and gas volumes on the Blake Ridge with electrically resistivity log data. Proc. Ocean Drilling Program, Scientific Results, v.164, pp.179-191.

Cook, A., Goldberg, E.D. and Kleinberg, R.L. (2008) Fracture- controlled gas hydrate systems in the northern Gulf of Mexico. Marine Petrol. Geol., v.25, pp.932-941.

Cook, A., Anderson, B., Malinverno, A., Mrozewski, S. and Goldberg, D. (2010) Electrical anisotropy due to gas hydrate-filled fractures: Geophysics, v.75(6), pp.173-185, doi: 10.1190/1.3506530.

Coffin, R., Pohlman, J., Gardner, J., Downer, R., Wood, W., Hamdan, L., Walker, S., Plummer, S., Gettrust, J., Diaz, J. (2007) Methane hydrate exploration on the mid Chilean coast: a geochemical and geophysical survey. Jour. Petrol. Sci. Engg., v.56, pp.32-41.

Dvorkin J., Prasad, M., Sakai, A. and Lovoie, D. (1999) Elasticity of marine sediment: Rock Physics modeling. Geophys. Res. Lett., v.26(12), pp.1781-1784.

Fertl, W. and Frost, E. (1980) Evaluation of shalyclastic reservoir rocks. Jour. Petrol. Tech., September, pp.1641-1645

Fofonoff, N.P. (1985) Physical properties of seawater: a new salinity scale and equation of state for sea water. Jour. Geophys. Res., v.90, pp.3332-3342.

Fuloria, R.C., Pandey, R.N., Bharali, B.R., and Mishra, J.K. (1992) Stratigraphy, Structure and Tectonics of Mahanadi offshore basin in: recent geoscientific studies in the Bay of Bengal and the Andaman basin. Jour. Geol. Soc. India, v.29, pp.255-265.

Gassmann, F. (1951) Elasticity of porous media, Vierteljahrsschrifi der Naturforschenden Gesselschaft, v.96, pp.1-23.

Ghosh, R., Kalachand, S. and Ojha, M. (2010) Effective medium modeling of gas hydrate filled fractures using the sonic log in the Krishna-Godavari basin, offshore eastern India. Jour. Geophys. Res., v.115, B06101, doi: 10.1029/2009JB006711.

Hashin Z., and Shtrikman S. (1963) A variational approach to the elastic behavior of multiphase materials. Jour. Mech. Phys. Solids, v.11(2), pp.127-140

Helgrude M. B., Dvorkin J., A. Nur, A. Sakai, and T. Collett, (1999) Elastic wave velocity in marine sediments with Gas hydrates: Effective medium modeling, Geophys. Res. Lett., 26(13), 2021-2024.

Hill R. (1952) The elastic behavior of crystalline aggregate, Proc. Physical Soc., London, A65, pp.349-354.

Kumar, D., Sen, M.K., Bangs, N.L., Wang, C. and Pecher, I. (2006) Seismic anisotropy at Hydrate Ridge: Geophys. Res. Lett., v.33, L01306, doi: 10.1029/2005GL023945.

Kumar, P., Collett, T. S., Boswell, R., Cochran, J. R., Lall, M., Mazumdar, A., Ramana, M. V., Ramprasad, T., V, M., Sain., K., Sathe, A. V., Vishwanath, K. and Yadav, U.S. (2014) Geologic implications of gas hydrates in the offshore of India: Krishna Godavari Basin, Mahanadi Basin, Andaman Sea, Kerala Konkan Basin, Marine Petrol. Geol., v.58, pp.29-98.

Lee, M.W., Hutchinson, D.R., Collett, T.S. and Dillon, W.P. (1996) Seismic velocities for hydrate-bearing sediments using weighted equations. Jour. Geophys. Res.: Solid Earth, v.101(B9), pp.20347-20358.

Lee, M.W. and Collett, T.S. (2011) Three types of gas hydrate reservoirs in the Gulf of Mexico identified in LWD data. *In:* 7th Internat. Conf. Gas Hydrates (ICGH 2011).Endinburgh, Scotland, UK, July 17-21, P-39

Lee, M.W. and Collett, T.S. (2012) Pore-and fracture-filling gas hydrate reservoirs in the Gulf of Mexico gas hydrate joint industry project leg II Green Canyon 955 H well. Marine Petrol. Geol., v.34(1), pp.62-71.

Miller, J. J., Lee, M. W., and von Huene, R. (1991) An Analysis of a Seismic Reflection from the Base of a Gas Hydrate Zone, Offshore Peru (1). AAPG Bull., v.75(5), pp.910-924.

Mavko G., T.Mukerji, and Dvorkin J. (2009) The rock physics handbook, 2nd edition: Cambridge University Press. doi:10.1017/CBO9780511626753.

Murphy, W.F., 1982, Effects of Microstructure and Pore Fluids on the Acoustic properties of Granular Sedimentary Materials. Ph.D. Dissertation Stanford University, June 1982.

Nobes, D. C., Villinger, H., Davis, E. E., and Law, L. K. (1986) Estimation of marine sediment bulk physical properties at depth from seafloor geophysical measurements. Jour. Geophys. Res.: Solid Earth, v.91(B14), pp.14033-14043.

Pandey, L, Sain, K, Joshi, A. K. (2019) Estimate of gas hydrate saturations in the Krishna-Godavari basin, eastern continental margin of India, results of expedition NGHP-02, Marine and Petroleum Geology doi: 10.1016/j.marpetgeo.2018.12.009.

Rai, N, Singha, D.K., Shukla, P.K. and Sain, K. (2020) Delineation of discontinuity using multi-channel seismic attributes: An implication for identifying fractures in gas hydrate sediments in offshore Mahanadi basin, Result in Geophysical Science, pp.1-4, 100007.

Reuss, A. (1929) Berechnung der Fliessgrenzev von Mischkristallen auf Grund der Plastizittitsbedingung fur Einkristalle, Ztschr. fur Angewandte Math. u. Mech., v.9, pp.49-58.

Sain, K. and Gupta, H.K. (2012) Gas hydrates in India: potential and development. Gondwana Res., v.22, pp.645-657.

Sain, K., Rajesh, V., Satyavani, N., Subbarao, K.V. and Subrahmanyam, C. (2011) Gas-hydrate stability thickness map along the Indian continental margin; Marine Petrol. Geol., v.28, pp.1779-1786.

Satyavani, N., Sen, M.K. and Sain, K. (2013) Azimuthal anisotropy from OBS Observation in Mahanadi offshore, India, Interpretation, v.1(2), pp.187-198.

Sastri, V.V., Sinha, R.N., Singh, G., Murti, K.V.S. (1973) Stratigraphy and tectonics of sedimentary basins on the east coast of penninsular India. AAPG Bull., v.57, pp.655-678.

Sastri, V.V., Venkatachala, B.S., Narayanan, V. (1981) The evolution of the east coast of India. Palaeogeo. Palaeoclimat. Palaeoecol., v.36, pp.23-54.

Sayers, C. M. and Kachanov, M. (1995) Microcrack-induced elastic wave anisotropy of brittle rocks: Jour. Geophys. Res., v.100, pp.4149-4156, doi: 10.1029/94JB03134.

Serra, O. (1984) Fundamentals of Well-Log Interpretation (Vol. 1): The Acquisition of Logging Data. Developments in Petroleum Science. 15A. Amsterdam: Elsevier.

Shankar, U., Gupta, D.K., Bhowmick, D., Sain, K. (2013) Gas hydrate and free gas saturations using rock physics modelling at site NGHP 01-05 and NGHP 01-07 in the Krishna-Godavari Basin, eastern Indian margin, Jour. Petrol. Sci. Engg., v.106, pp.62-70.

Shankar, U and Pandey, A.K. (2019) Estimation of gas hydrate saturation using isotropic and anisotropic modelling in the Mahanadi basin. Jour. Earth System Sci., v.128, pp.163.

Shukla, P. K., Singha, D.K. and Sain, K. (2022a) Anisotropy analysis in shallow marine gas hydrate bearing sediments: A case study from the offshore Mahanadi basin, India. Marine Geophys. Res., v.43(3)

Shukla, P.K., Singha, D.K., and Sain, K., (2022b) Modeling of in-situ horizontal stresses and orientation of maximum horizontal stress in the gas hydrate-bearing sediments of the Mahanadi offshore basin, India. Geomech. Geophys. Geo-energ. Geo-resour., v.8, pp.90, 1-21. doi:10.1007/s40948-022-00401-6

Singha, D.K., Shukla, P.K., Chatterjee, R., and Sain, K. (2019) Multi- Channel 2D Seismic Constraints on Pore Pressure- and vertical stress- related Gas Hydrate in the deep offshore of the Mahanadi Basin, India, Jour. Asian Earth Sci., v.180, 103882.

Singha, D.K., Chatterjee.R., Sen, M.K. and Sain, K. (2015) Pore Pressure Prediction in Gas-Hydrate bearing Sediments of Krishna-Godavari Basin, India, Marine Geol., v.357, pp.1-11

Sloan J.E.D. (1998) Clathrate hydrates of natural gases, 2nd edn. Dekker, New York.

Stoll, R.D. andBryan G.M. (1979) Physical properties of sediments containing gas hydrate. Jour. Geophys. Res., v.84(B4), pp.1629-1634.

Tucholke, B.E, Bryan, G.M, Ewing, J.I. (1977) Gas-hydrate horizons detected in seismic-profiler data from the western North Atlantic. AAPG Bull., v.61, pp.698-707

Waite, W.F., Ruppel, C.D., Collett, T.S., Schultheiss, P., Holland, M., Shukla, K.M., Kumar, P. (2019) Multi-measurement approach for establishing the base of gas hydrate occurrence in the Krishna-Godavari Basin for sites cored during expedition NGHP-02 in the offshore of India. Jour. Marine Petrol. Geol., v.108, pp.296-320.

Wood, W.T., Stoffa, P.L. and Shipley, T.H. (1994) Quantitative Detection of Methane Hydrate through High-Resolution Seismic Velocity Analysis. Jour. Geophys. Res.: Solid Earth, v.99, pp.9681-9695. doi.org/10.1029/94JB00238

Wood, A.B. (1941) A text Book of Sound: being an account of the physics of the vibrations with special reference to recent theoretical and technical developments, Macmillan, New York.